Research Square

Preprints are preliminary reports that have not undergone peer review.
They should not be considered conclusive, used to inform clinical practice,
or referenced by the media as validated information.

Numerical Investigation of Chemical Reaction and Thermal Radiation Effects on MHD Williamson Nanofluid Flow over a Hyperbolic Tangential Stretching Sheet with Joule Heating

Ramesh Kune

ramesh.k@sreenidhi.edu.in

Sreenidhi Institute of Science and Technology

Hari Singh Naik Sabawat

Osmania University

Research Article

Keywords: Williamson fluid, suctions Joule heating and radiation parameter

Posted Date: November 2nd, 2026

DOI: https://doi.org/10.21203/rs.3.rs-11299894/v1

License: This work is licensed under a Creative Commons Attribution 4.0 International License.
Read Full License

Additional Declarations: No competing interests reported.

Numerical Investigation of Chemical Reaction and Thermal Radiation Effects on MHD Williamson Nanofluid Flow over a Hyperbolic Tangential Stretching Sheet with Joule Heating.

Ramesh Kune[1]*, Hari Singh Naik Sabawat[2]

1.Department of Mathematics, Sreenidhi Institute of Science and Technology, Ghatkesar, Hyderabad, Telangana 501301, India

2. Department of Mathematics, Osmania University, Hyderabad-500007, Telangana, India

Abstract:

This work justifies a thorough examination of the combined impacts of Joule heating and suction parameter on the chemically reactive Non-Newtonian Nanofluid flow through a tangent hyperbolic permeable sheet. In order to provide a more representative image of the physical events, the study takes into account the parameters of thermal radiation and suction parameter. By applying similarity transformations, altered the governed nonlinear PDEs are renewed to a set of differential equations. The R-K method is used to handle these altered equations numerically. The findings demonstrate the important regulation of joule heating and suction parameter. The escalation in joule heating upsurges the temperature, whereas suction depreciates the velocity and temperature. Moreover, the velocity, concentration and temperature distributions are significantly impacted by the addition of thermal radiation and velocity slip. According to parametric studies, the current system is validated against changes in the thermophoresis, radiative heat, Brownian motion, and Williamson fluid parameters.

Keywords: Williamson fluid, suctions Joule heating and radiation parameter.

Findings:

The primary objective of the study as follows:

To scrutinize the role of suction parameter with the joule heating on the concentration and temperature profiles in hyperbolic Williamson nanofluid flow along a permeable sheet.

To evaluate the impact of various factors on heat and mass transfer rate and skin friction.

Introduction:

MHD is playing crucial role in thermoelectric power energy, coating of cable, refrigeration objects and thermal storage. This type of research is very important for dialysis equipment refrigeration and medical devices. Das et.al [1, 2, 3, 4] analyzed the MHD effect on Casson nanofluid past on vertical plate. Heat transfer characteristics of MHD Williamson fluid flow through an exponential porous sheet analyzed by Ahmed et.al [5]. Investigated the influence of MHD flow of a nanofluid with variable thermal conductivity and convective heating [6, 7]. Reddy MV et.al [8] studied the numerical treatment in Williamson MHD flow of the fluid with effect of Heat flux and suction parameter. Razaq et.al [9] fin out the effects of thermal radiative and heat source on MHD flow.

Non-Newtonian fluids with their different kind of characteristics and due to high demand researchers are focus to study on these fluids. Due to various types of rheological properties are made to be used in pharmaceutical, chemical and mechanical engineering. Nima et al. [10] examined the thermal effect on non-Newtonian steady mixed convicting flow of fluid along a vertical non-Darcy porous medium. Chinyoka T and Rajput et al. [11-12] investigated the unsteady flow of a variable viscosity fluid along the circular pipe. The multiple solutions of Casson nanofluid MHD flow along porous medium analyzed by Raza et al. [13]. The impact of entropy generation and suction parameter on MHD non-Newtonian nanofluid flow with the help of Successive linearization method studied by Qing et al. [14]. Homogeneous reactions with heat effect on on MHD stagnation point flow studied by Khan et al. [15]. Loganathan et al. [16] analyzed the effect of thermal radiation on Casson electromagnetic fluid in a Riga-plate.

The Williamson fluid performed as non-Newtonian which reveals behaviour, like a shear thinning liquid. Where viscosity depreciate in the presence of shear stress. The entropy generation and chemical reactions effects in were investigated by Nadeem Sohail et al. [17]. Khan et al. [18] investigated the chemical reactions impact on non-Newtonian Williamson fluid in a boundary layer film system. Hashim et al. [19] studied influence of heat source/sink of Williamson nanofluid passing through the wedge- geometry plate. The impact of radiation and thermal diffusion on the Williamson fluid was investigated by Refs. [20, 21]. Yusuf TA et al. [22] investigated the effect of Lorenz force and heat radiation with variable viscosity on Williamson fluid flow.

The suction parameter is crucial for understanding and controlling how suction affects fluid flow near surfaces. It is applications range from aerospace to thermal engineering and environmental systems. By adjusting suction, engineers can optimize performance, reduce drag, enhance heat transfer, and maintain flow stability. Sakiadis [23] studied the boundary layer flow on the stretching continuously varying stretching sheet. Shahid khan et.al [24] studied the 3-Dimesional carreau fluid flows along the stretching sheet in the account of mass and heat transfer. There is a significant work done on the nanofluids are passing throw on the stretching sheet by the researchers [25, 26, 27, 28 &31]. The impact of suction or injection on the steady flow of nanofluid across an exponential sheet discussed by M. Radhika et al [29**]**. Chowdepalli et.al [30] examined the suction parameter influences on the impact of soil compaction behavior and heat transfer rate.

Thermal radiation is the process where electromagnetic waves transfer thermal energy from a hotter object to a cooler object, without needing a medium like air or water. It plays a significant role in boundary layer theory, particularly in high-temperature environments and we need to study the effect of radiative heat transfer on a fluid flow. Radiation heat transfer occurs when thermal radiation is produced by a temperature difference between the fluid and a sheet it. This effect becomes greater in fluids with stronger radiative properties or at higher temperatures. Total heat transfer might be affected if nanoparticles alter the base fluid's radiative properties. Gnaneswara Reddy et al. [32,33] investigated the impact of Brownian motion and heat radiation parameter on

laminar fluid flow. The thermal radiation and heat transfer properties on an electrically conductive fluid flow near isothermal sheet by AboEldahab, EM [34. 35].

Research gap

In the above literature all are studied the non-Newtonian Williamson fluid with combination tangential hyperbolic fluid flow with effect of thermal radiation and stretching parameter but not focused on joule effect (neglected the ohmic dissipation). In MHD nanofluid flow Magnetic field via joule heating play a vital role. The electrical energy converts magnetic parameter via joule heating, which help us understand boundary layer thickness and thermal properties of the surface. And also in the present work Williamson fluid consider that it has a constant chemical properties and examination is done on mass and heat transfer mechanism over a stretching sheet and is situated in a porous medium. We solved nonlinear partial differential equations with appropriate similarity transformation and evolved with RK method bvp4c technic.

Mathematical Modeling

In the present study, we consider a steady of 2-Dimensional nanofluid flow exhibiting a hyperbolic tangent hyperbolic fluid model, accounting for variable thermal conductivity, as it flows over a nonlinearly stretching plate. The sheet is situated along side of the x-axis, while the y-axis is taken vertical to it. The fluid motion is induced by the stretching plate, and the flow is assumed to be confined the region $y > 0$. The physical configuration of the problem is illustrated schematically in Figure 1.

A transversal magnetic field of strength B is applied along the y-direction. The sheet stretches via the direction of X-axis in this direction velocity is given by

$$u_w = ax^{1/3},$$

Where ‘a’ is a positive constant. The applied magnetic field is

$$B = B_0 x^{-2/3}.$$

The analysis combines both mass and heat transfer phenomena, including the impact of a chemical reaction considered by the reaction rate constant K. Heat radiation are also taken into account, with the radiative heat flux. The stretching sheet is inserted in a porous medium, and the fluid flow within this medium is governed by Darcy’s law. Furthermore, thermophoresis effects are included to account for nanoparticle transport induced by temperature gradients.

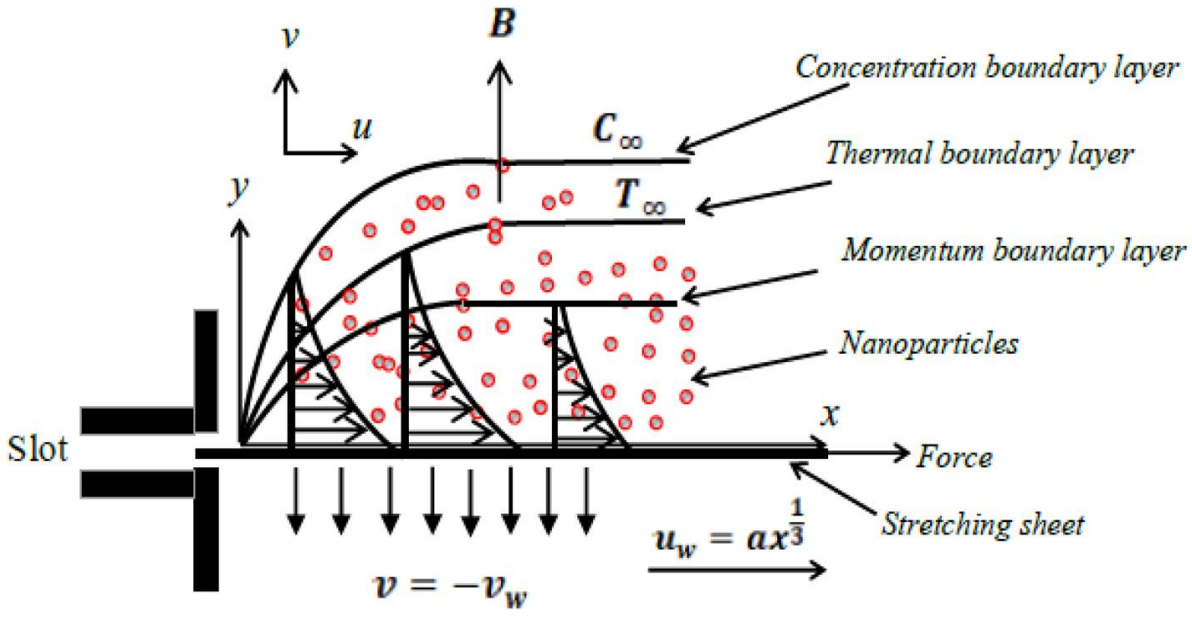


Fig 1.Geometrical representation

$$\frac{\partial u^*}{\partial x^*}+\frac{\partial v^*}{\partial y^*}=0. \tag{1}$$

$$u^*\frac{\partial u^*}{\partial x^*}+v^*\frac{\partial u^*}{\partial y^*}=\frac{\mu}{\rho}\left[(1-n)\frac{\partial^2 u^*}{\partial y^{*^2}}+\sqrt{2\upsilon}\Gamma\frac{\partial u^*}{\partial y^*}\frac{\partial^2 u^*}{\partial y^{*^2}}\right]-\frac{\sigma B^2 u^*}{\rho}-\frac{\mu u^*}{\rho k}. \tag{2}$$

$$u^*\frac{\partial T^*}{\partial x^*}+v^*\frac{\partial T^*}{\partial y^*}=\frac{1}{\rho c_p}\frac{\partial}{\partial y^*}\left(k(T)\frac{\partial T^*}{\partial y^*}\right)-\frac{1}{\rho c_p}\frac{\partial q_r}{\partial y^*}+\tau\left[\frac{D_T}{T_\infty^*}\left(\frac{\partial T^*}{\partial y^*}\right)^2+D_B\frac{\partial C^*}{\partial y^*}\frac{\partial T^*}{\partial y^*}\right]+$$
$$\frac{\mu}{\rho c_p}\left[(1-n)\left(\frac{\partial u^*}{\partial y^*}\right)^2+\frac{n}{\sqrt{2}}\Gamma\left(\frac{\partial u^*}{\partial y^*}\right)^3\right]+\frac{\sigma B^2\left(u^*\right)^2}{\rho c_p}. \tag{3}$$

$$u^*\frac{\partial C^*}{\partial x^*}+v^*\frac{\partial C^*}{\partial y^*}=\frac{D_T}{T_\infty^*}\frac{\partial^2 T^*}{\partial y^{*^2}}+D_B\frac{\partial^2 C^*}{\partial y^{*^2}}-K_0\left(C^*-C_\infty^*\right). \tag{4}$$

$$As\ y^*=0,\ v^*=-v_w, u^*=u_w(x)=ax^{\frac{1}{3}},\ C^*=C_w^*,\ T^*=T_w^*, \tag{5}$$

$$y^*\to\infty,\quad u^*\to u_w(x)=0, C^*\to C_\infty^*,\ T^*\to T_\infty^*,$$

The transformations

$$\eta = \frac{1}{x^{\frac{1}{3}}}\sqrt{\frac{a}{v}}y^*, \quad u^* = ax^{\frac{1}{3}}f'(\eta), \quad v = -\frac{\sqrt{av}}{3x^{\frac{1}{3}}}(2f(\eta) - 3f'(\eta), \quad \theta(\eta) = \frac{T^* - T_\infty^*}{T_w^* - T_\infty^*}, \quad \phi(\eta) = \frac{C^* - C_\infty^*}{C_w^* - C_\infty^*}.$$

$$k = k_\infty(1 + \varepsilon\theta), \tag{6}$$

$$\frac{1}{\Pr}\left((1 + R + \varepsilon\theta)\theta'' + \varepsilon\theta'^2\right) + b\theta'\phi' + \delta_t\theta'^2 + \frac{2f\theta'}{3} + Ec\left[(1-n)f''^2 + \frac{n\Gamma_e}{2}f''^3\right] + J\left(f'\right)^2 = 0.$$

$$\left(n\Gamma_e f'' + (1-n)\right)f''' - \frac{f'^2}{3} + \frac{2ff''}{3} - \left(M + k_p\right)f' = 0. \tag{7}$$

$$\frac{1}{\Pr}\left((1 + R + \varepsilon\theta)\theta'' + \varepsilon\theta'^2\right) + b\theta'\phi' + \delta_t\theta'^2 + \frac{2f\theta'}{3} + Ec\left[(1-n)f''^2 + \frac{n\Gamma_e}{2}f''^3\right] + J\left(f'\right)^2 = 0. \tag{8}$$

$$\phi'' + \frac{2}{3}Scf\phi' + \frac{\delta_t}{b}\theta'' - k\phi = 0. \tag{9}$$

Following to the following

$$\begin{aligned} f &= f_w, \quad f' = 1, \quad \theta = 1, \quad \phi = 1, \quad at \quad \eta = 0, \\ f' &= 0, \quad \theta = 0, \quad \phi = 0, \quad as \quad \eta \to \infty. \end{aligned} \tag{10}$$

The governing parameters are defined as follows:

$$k_p = \frac{vx^{\frac{1}{3}}}{ak}, \quad f_w = \frac{3v_0}{2\sqrt{av}}, \quad M = \frac{\sigma B_0^2}{a\rho}, \quad \Gamma_e = \frac{\sqrt{2}a^{\frac{3}{2}}x\Gamma}{\sqrt{v}}, \quad Ec = \frac{u_w^2}{c_p\left(T_w^* - T_\infty^*\right)}, \quad J = Ec * M$$

$$\delta_t = \frac{\tau D_B\left(C_w^* - C_\infty^*\right)}{v}, \quad R = \frac{16\sigma^* T_\infty^*}{3kk^*}, \quad b = \frac{\tau D_B\left(C_w^* - C_\infty^*\right)}{v}, \quad Sc = \frac{v}{D_B}, \quad k = \frac{kx^{\frac{2}{3}}}{a}, \quad \Pr = \frac{\mu c_p}{k_\infty}.$$

$$\begin{aligned} \mathrm{Re}_x^{\frac{-1}{2}}\, Sh_x &= -\phi'(0), \qquad \mathrm{Re}_x^{\frac{-1}{2}}\, Nu_x = -\theta'(0), \\ \mathrm{Re}_x^{\frac{-1}{2}}\, Cf_x &= -\left[(1-n)f''(0) + \frac{n\Gamma_e}{2}f''^2(0)\right]. \end{aligned} \tag{11}$$

Where $\mathrm{Re}_x = \frac{xu_w}{v}$.

Method of solution

The convergence and stability on the based, Runge - Kutta method for solving the transformed nonlinear ordinary differential equations and pictorial graphs by MATLAB.

$$f = \aleph_{1,} \quad f' = \aleph_2, \quad f''' = \aleph_3,$$
$$\theta = \aleph_{4,} \quad \theta' = \aleph_{5,} \quad \phi = \aleph_{6,} \quad \phi' = \aleph_7. \tag{12}$$

The set of Equations.(6) - (9) are reduced to

$$\aleph_1' = \aleph_2, \quad \aleph_1(0) = f_w,$$
$$\aleph_2' = \aleph_3, \quad \aleph_2(0) = 1,$$
$$\aleph_3' = \frac{\frac{\aleph_2^3}{3} + \left(M + k_p\right)\aleph_2 - \frac{2}{3}\aleph_3\aleph_1}{n\Gamma_e\aleph_3 + (1-n)}, \quad \aleph_3(0) = \chi_1,$$
$$\aleph_4' = \aleph_5, \quad \aleph_4(0) = 1,$$
$$\aleph_5' = \frac{-\varepsilon\aleph_5^2 + \Pr\left[-b\aleph_5\aleph_7 - \delta_t\aleph_5^2 - -\frac{2}{3}\aleph_5\aleph_1 - Ec\left((1-n)\aleph_3^2 + \frac{n\Gamma_e}{2}\aleph_3^3\right) + J\left(\aleph_2\right)^2\right]}{(1 + R + \varepsilon\aleph_4)}, \quad \aleph_5(0) = \chi_2,$$
$$\aleph_6' = \aleph_7, \quad \aleph_6(0) = 1,$$
$$\aleph_7' = -\frac{2}{3}Sc\aleph_1\aleph_7 - \left(\frac{\delta_t}{b}\right)\aleph_5' + k\aleph_6, \quad \aleph_7(0) = \chi_3,$$
$$when \quad n \to \infty$$
$$\aleph_2 \to 0, \quad \aleph_4 \to 0, \quad \aleph_6 \to 0$$

To estimates the $\chi_1, \chi_{2,}$ *and* χ_3, the shooting method is used and ensuring the appropriate boundary conditions $\aleph_2(\infty), \aleph_4(\infty)$, and $\aleph_6(\infty)$. This process can be continue until the desired level of accuracy, specifically 10^{-6}, is attained.

Results and discursions

In fig 2. Thermophoresis states the drive of suspended particles from a hot region toward a colder region under the influence of a temperature gradient. This phenomenon plays an important role in nanofluid transport processes. As escalate the thermophoresis parameter (δ_t), the thermal energy carried by nanoparticles migrating away from the heated region upsurges. Consequently, more heat is transported into the fluid region, which leads to rise in the temperature fluid. The enriched thermophoretic force declines the temperature at the wall, resulting in decay in the heat transfer rate. And same results noticed in concentration profile.

Fig.3. illustrates the influence of Brownian motion effect on concentration and temperature. Brownian motion states the arbitrary drive of nanoparticles suspended in a Nano fluid, which caused by continuous collisions between fluid molecules and nanoparticles of the fluid. Unlike

thermophoresis, Brownian motion is not driven by a temperature gradient, but by irregular movement of fluid particles.

As Brownian motion values **(**Nb) upsurges, the random motion of nanoparticles strengthens, which augments transformation of energy between the base fluid and the nanoparticles**.** This increased interaction leads to a growth in the fluid temperature and causes improve the thickness of the thermal boundary layer**.** Consequently, the temperature gradient at the surface decreases, resulting in a reduction in the surface heat transfer rate.

Fig. 4 & 5. Illustrates the impact of power - law index (n) on the velocity, concentration and heat profiles. It is observed that growing 'n' leads to a noticeable decay in the velocity profile due to greater viscous resistance of the fluid. In contrast, the concentration and temperature profiles increase with increasing n, accompanied by a thickening of the corresponding concentration and thermal boundary layers. This behavior is endorsed to the suppression of convective transport caused by higher effective viscosity at larger values of the power-law index.

Fig. 6-7. Shows the effect of the suction parameter on velocity, concentration and temperature. Suction refers the strength of the fluid removal towards the surface, the elevated 'f_w' values the reduction in nanofluid velocity is observed in the graphs, which caused by porous resistance to the fluid flow. In the same pattern occurs in temperature and concentration profile as increases the values of suction parameter.

The thermal radiation parameter influence the dimensionless temperature factor is presented in Fig. 8. It is clearly noticed an increase in the thermal radiation profile leads to a notable upsurge in the temperature distribution within the thermal boundary layer. This occurs because thermal radiation enhances the overall transport of heat energy within the fluid, thereby growing fluid temperature. Physically, stronger thermal radiation contributes additional energy to the flow field in the form of radiative heat flux, which elevates the temperature of the fluid near the stretching sheet and t the boundary layer region.

Fig. 9 The Joule heating arises due to the conversion of electrical energy into thermal energy when an electrically conducting fluid flows under the influence of a magnetic field. As the Joule heating parameter increases**,** the electrical current induced within the fluid intensifies, leading to a greater generation of internal heat. Consequently, additional thermal energy is released into the fluid, which causes a rise in the temperature profile throughout the boundary layer. This increase in internal heat generation results in the thickness of the thermal boundary layer and a reduction in the temperature gradient near the wall.

The temperature profile demonstrates an enhancement as the Eckert number enhances, as illustrated in Fig. 10. The physical explanation is that an increase in Ec may cause the fluid's viscosity to absorb more energy, which it can then transform into internal energy, therefore raising the temperature.

Fig.11-12. Increase in the chemical reaction profile slightly decreases the velocity distribution across the boundary layer and escalations in temperature and concentration. This behavior is attributed to the decline in nanoparticle concentration caused by the chemical reaction, which alters

the effective fluid viscosity and density. As a result, the thickness of the momentum boundary layer decreases marginally with growing values of K.

Temperature Profile: It shows a noticeable increase with increasing chemical reaction parameter. This enhancement occurs because chemical reactions may release heat (exothermic reaction), thereby adding thermal energy to the system. Consequently, the thermal boundary layer becomes thicker, and the fluid temperature

upsurges near the stretching sheet and throughout the flow domain.

Concentration profile: The concentration distribution decreases significantly as the chemical reaction parameter escalates. A stronger chemical reaction accelerates the consumption of species, leading to a rapid decline in concentration. This results in a thinner concentration boundary layer and concentration gradient at the surface, which boosts the mass transfer rate.

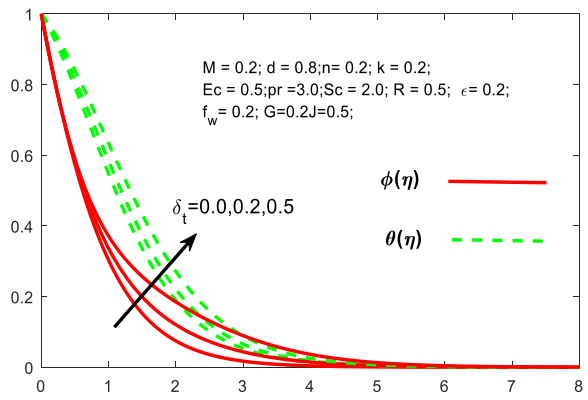


Fig 2. δ_t effect on temparature and concentration

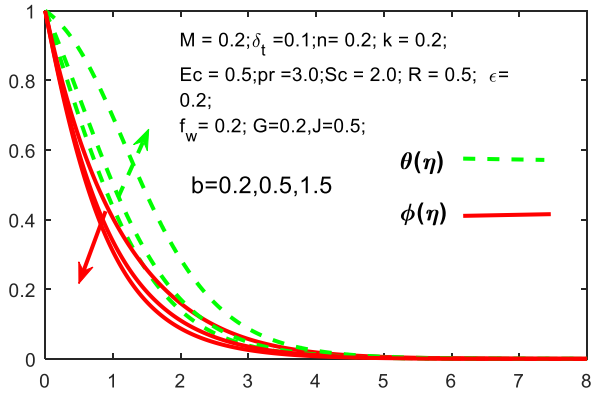
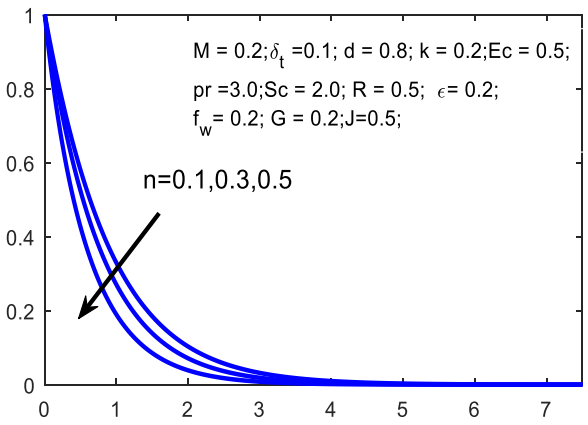


Fig 3. b effect on temparature and concentration



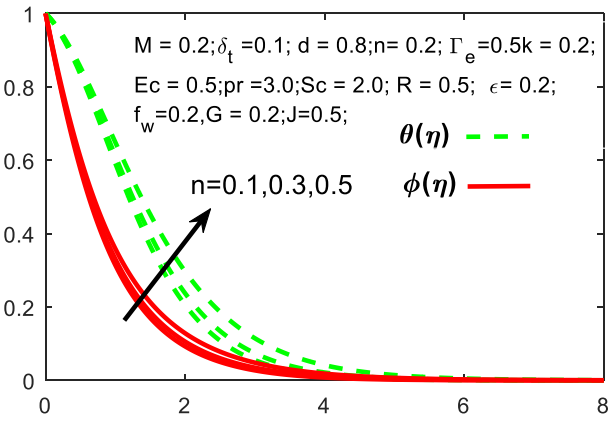


Fig 4. n Effect on Velocity

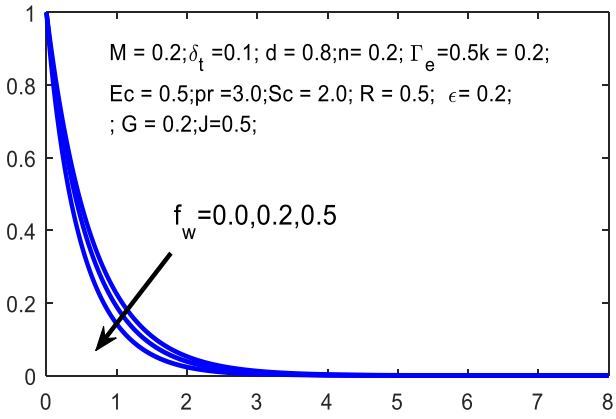


Fig 5. n Effect on Temperature and concentration

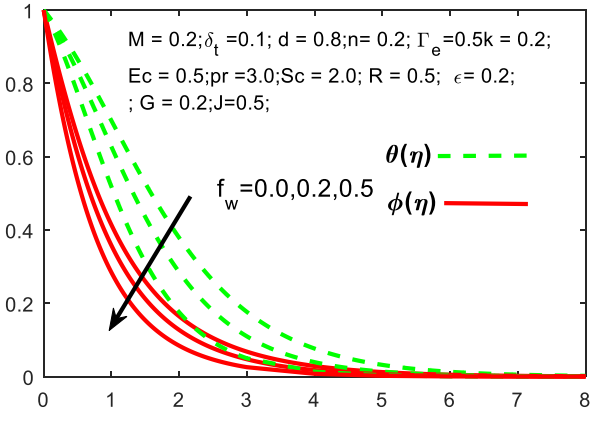
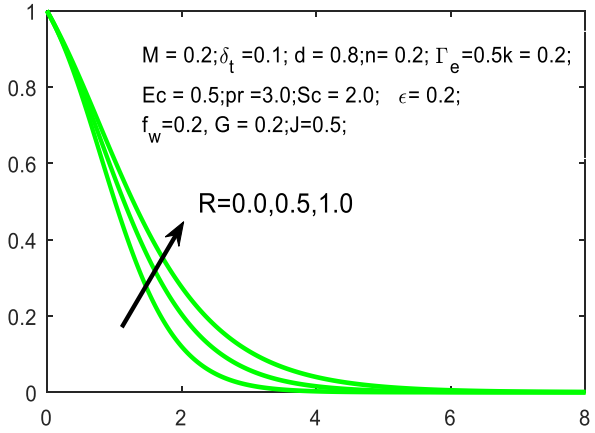


Fig 6. f_w effect on Velocity

Fig 7. f_w effect on concentration andTemperature



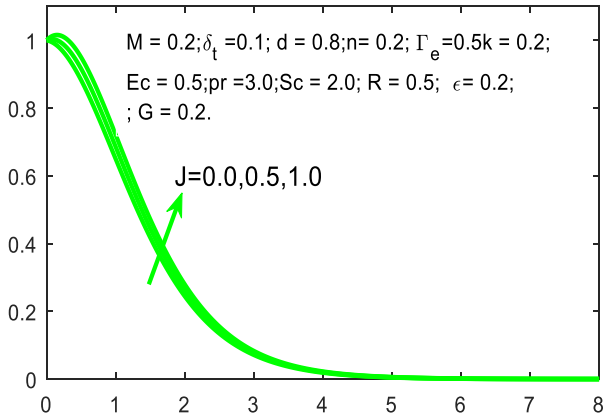
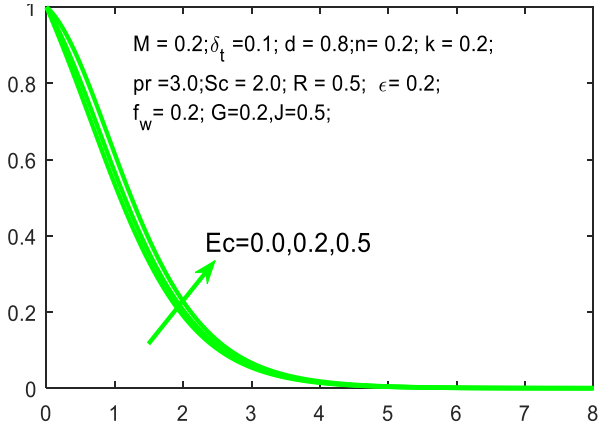
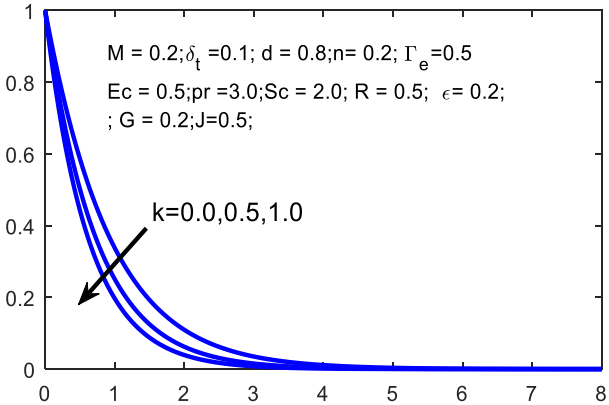


Fig 8. R vs Temperature

Fig 9. J vs Temperature





.Fig 10. Ec vs Temperature

Fig 11. k vs Velocit

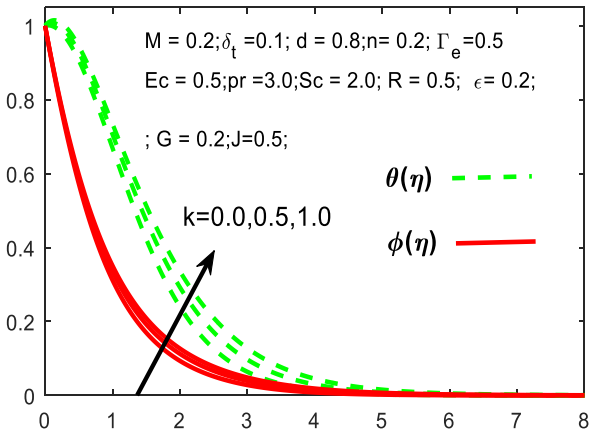


Fig 12. k vs Temperature and concentration

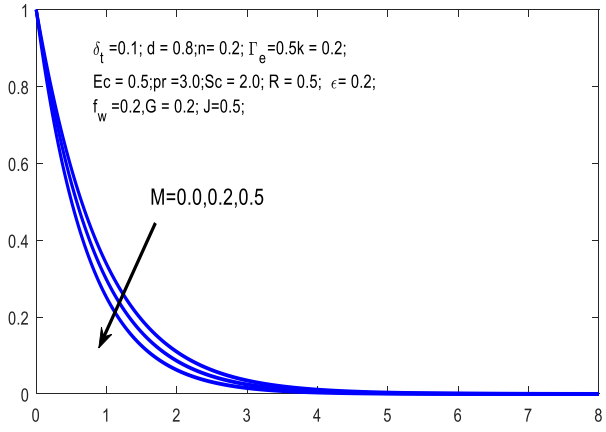


Fig 13.M vs Velocity

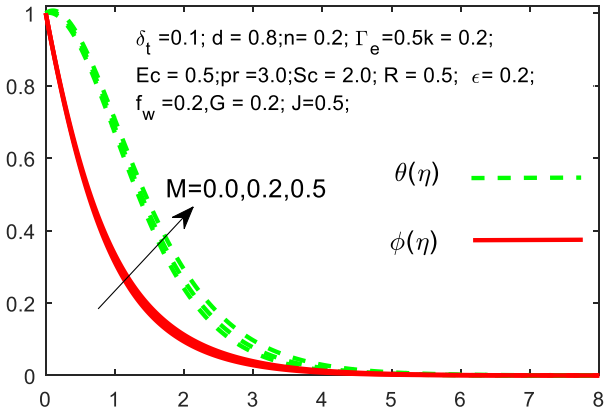


Fig 14. M vs Temperature and Concentration

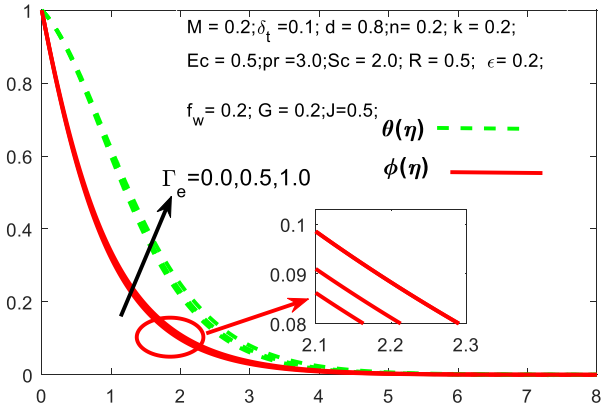


Fig 15. Williamson vs temperature and concentration

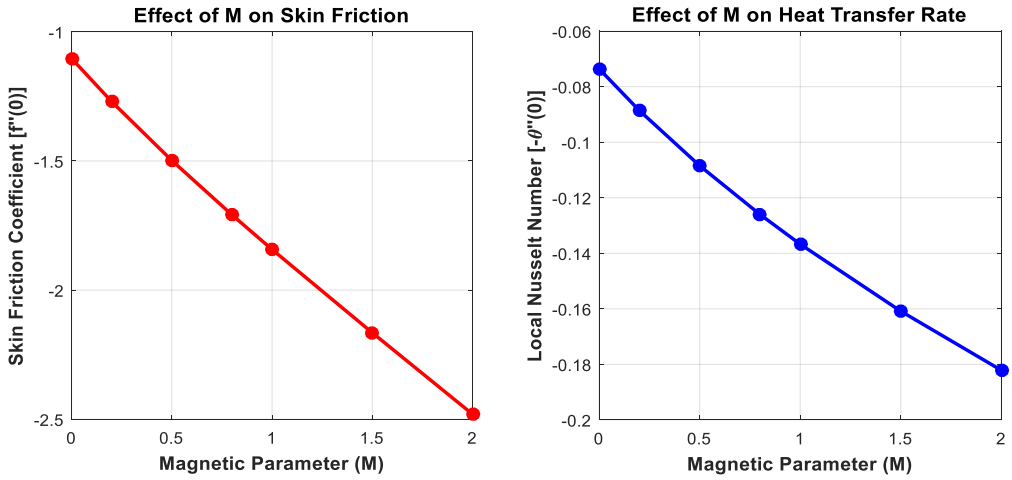


Fig 16. Magenetic field vs skin fricktion and heat transfer rate

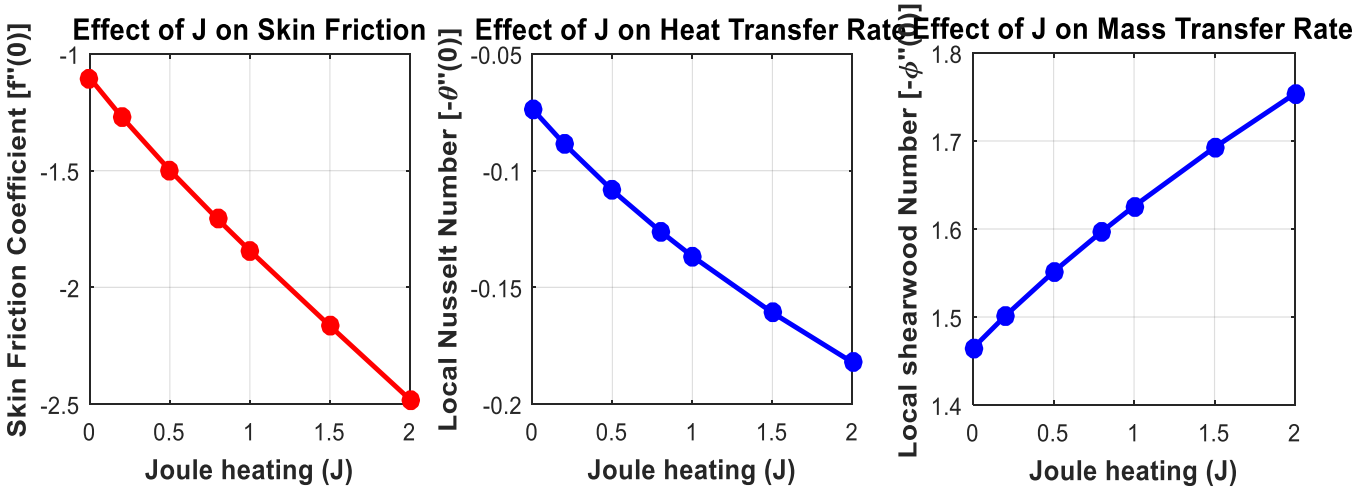


Fig 17. Joule heating vs skin fricktion, mass and heat transfer rate

The influence of the magnetic parameter M on the temperature, velocity and concentration profiles is illustrated in Fig.(13-14).

Velocity Profile:

It is noticed that a rise in the magnetic profile leads to a reduction in the velocity distribution within the boundary layer. Physically, the transverse magnetic field generates a Lorentz force that works opposite to the direction of the flow, thereby slowdown the fluid motion. This magnetic damping effect reduces the velocity of the fluid and causes a reduction in the momentum boundary layer thickness.

Temperature Profile: The temperature profile upsurges with increasing magnetic parameter. The reduction in velocity due to the Lorentz force enhances the conversion of kinetic energy into thermal energy through Joule (ohmic) heating. As a result, additional heat is generated within the fluid, leading to a rise in temperature and an increase in the thermal boundary layer thickness.

Concentration Profile: An escalation in the magnetic parameter which leads to an enhancement in the concentration. The suppressed fluid motion caused by the magnetic field weakens mass diffusion away from the surface, allowing nanoparticles to gather near the stretching sheet. Accordingly, the mass boundary layer becomes thicker, and the concentration decays more slowly with distance from the wall.

Fig.15. The Williamson parameter (We) characterizes non-Newtonian behavior in Williamson fluids, often studied in nanofluid flows over surfaces, where higher values indicate stronger shear-thinning effects due to the ratio of relaxation time to fluid deformation rate.

Effects on Temperature

Increasing the Williamson parameter elevates temperature profiles in the fluid boundary layer. This occurs as higher We reduces velocity, enhancing frictional heating and thermal boundary layer thickness.

Effects on Concentration

Higher Williamson parameter values typically boost concentration profiles near surfaces, linked to improved mass transfer rates. However, interactions with parameters like Schmidt number can reduce concentration farther from the wall.

Fig.16–17. Illustrates skin friction, mass and heat transfer rate with magnetic field and joule heating parameter.

Conclusions

The present work shows the effect joule heating along with thermal radiation on the flow of Williamson nanofluid passing through hyperbolic tangential porous sheet. The parametric behavior on the various profiles are presented in the below.

Key Flow Impacts

Magnetic fields and porosity generate resistive Lorentz forces that decelerate velocity profiles, with suction further thinning boundary layers by drawing fluid toward the sheet. Slip conditions oppose velocity enhancement from higher non-Newtonian Williamson parameters, while power-law index n reduces velocity but thickens thermal and concentration layers due to increased viscous resistance.

Thermal Effects

Joule heating, thermal radiation, Brownian motion, and thermophoresis elevate temperature profiles by converting kinetic energy to heat, thickening the thermal boundary layer and reducing wall heat transfer rates. Higher magnetic parameter M boosts temperature via enhanced Ohmic heating from slowed flow, and thermal conductivity factor ε promotes heat diffusion.

Concentration Behavior

Chemical reactions deplete species, thinning concentration profiles and boosting mass transfer, though magnetic effects and Williamson parameter We accumulate nanoparticles near the surface for thicker layers. Thermophoresis enhances concentration via particle migration, countering Brownian motion's diffusive reduction.

The enhanced values of Williamson parameter increase the fluid velocity profile.

Thermal radiation along with thermophoresis and Brownian inspires temperature of the in suction parameter.

Table1: Comparison table of $\mathrm{Re}_x^{\frac{1}{2}} Cf_x$ with the past findings of Abbas et al. when M = $\Gamma_e = 0.5$ and $f_w = 0$.

	Ahmed et.al[36]	Abbas et .al [37]	Present work
0	0.932196	0.932163	0.932155
1	1.016643	1.0166389	1.016644
2	1.096308	1.096307	1.096306

Table2: Shows the skin friction , Nusselt number and shear wood values with various parameter M,R,Ec,J,Sc, and n

M	R	f_w	Ec	J	Sc	δ_t	Γ_e	b	ε	n	Pr	$-Cf$	$-Nu_x$	$-Sh_x$
0.0	0.2	0.2	0.5	0.1	0.7	0.1	0.5	0.8	0.2	0.2	3	1.1031	0.0815	1.0215
0.5												1.4886.	0.0314	0.9892
1.0												1.8336	0.0123	0.9671
	0.0											1.265094.	0.071996	1.000972.
	0.5											1.265094	0.091552	0.997495.

		0.0										1.142320.	0.007204	0.840231.
		0.5										1.478818.	0.101019	1.281041.
			0.0									1.478818	0.405655	1.246244
			1.0									1.478818	0.205166	1.316032
				0.0								1.478818	0.101019	1.281041
				0.5								1.478818	0.005016	1.276350

REFERENCES:

1. Das, S, Ali, A, Jana, RN. Darcian slip flow of rotating magnetoreactive peg conveying MoS2 Casson nanofluid with ramped temperature and concentration. Spec Top Rev Porous Media Int J 2020;11:71–102. https://doi.org/10.1615/specialtopicsrevporousmedia.2020030547.

2. Ali, A, Jana, RN, Das, S. Radiative CNT-based hybrid magneto-nanoliquid flow over an extending curved surface with slippage and convective heating. Heat Transf 2020;50:2997–3020. https://doi.org/10.1002/htj.22015.

3. Das, UJ. MHD mixed convective slip flow of Casson fluid over a porous inclined plate with Joule heating, viscous dissipation and thermal radiation. *Int J Appl Math Comput Sci* 2021;11:3263–75. https://doi.org/10.28919/jmcs/5713.

4. Das, UJ, Majumdar, NM. A study of magnetohydrodynamic flow on a channel with induced magnetic field, Soret effect and heat radiation. *ZAMM J Appl Math Mech* 2023;103:e202200624.Search in Google Scholar.

5. Ahmed, K, Akbar, T, Muhammad, T, Alghamdi, M. Heat transfer characteristics of MHD flow of Williamson nanofluid over an exponential permeable stretching curved surface with variable thermal conductivity. Case Stud Therm Eng 2021;28:101544. https://doi.org/10.1016/j.csite.2021.101544.

6. Rasheed, HU, Islam, S, Helmi, MM, Alsallami, SA, Khan, Z, Khan, I. An analytical study of internal heating and chemical reaction effects on MHD flow of nanofluid with convective conditions. *Crystals* 2021;11:1523. https://doi.org/10.3390/cryst11121523.Search in Google Scholar

7. Okechi, NF, Asghar, S, Charreh, D. Magnetohydrodynamic flow through a wavy curved channel. *AIP Adv* 2020;10:035114. https://doi.org/10.1063/1.5142214.Search in Google Scholar.

8. Reddy MV, Vajravelu K, Ajithkumar M, Sucharitha G, Lakshminarayana P. Numerical treatment of entropy generation in convective MHD Williamson nanofluid flow with Cattaneo–Christov heat flux and suction/injection. Int J Modelling Simul 2024 Sep 23:1–8. https://doi.org/10.1080/02286203.2024.2405714.

9. Razaq, A, Hayat, T, Khan, SA, Jamal, SS. Dynamic interaction of thermal radiation and chemically reactive MHD flow of rheological material invoking heat source. Case Stud Therm Eng 2025;75:107278. https://doi.org/10.1016/j.csite.2025.107278.

10. Nima NI, Salawu SO, Ferdows M, Shamshuddin MD, Alsenafi A, Nakayama A. Melting effect on non-Newtonian fluid flow in gyrotactic microorganism saturated nondarcy porous media with variable fluid properties. Applied Nanoscience. Oct 2020; Vol (10), pg no:3911–3924. http://dx.doi.org/10.1007/s13204-020-01491-y.

11.Chinyoka T, Makinde OD. Computational dynamics of unsteady flow of a variable viscosity reactive fluid in a porous pipe. Mechanics Research Communications,april 2010,vol. 37(3),pg:347-353. . http://dx.doi.org/10.1016/j.mechrescom.2010.02.007.

12. Rajput GR, Shamshuddin MD, Salawu SO. Thermosolutal convective nonNewtonian radiativeCasson fluid transport over a vertical plate propagated by Arrhenius kinetics with heat source/sink, Heat Transfer. Vol.50(3):pg no: 2829–2848.

13. Raza J, Rohni AM, Omar Z. Multiple solutions of mixed convective MHD casson fluid flow in a channel. Journal of Applied Mathematics. July 2016. http://dx.doi.org/10. 1155/2016/7535793.

14. Qing J, Bhatti MM, Abbas MA, Rashidi MM, Ali M El. Entropy generation on MHD cassonnanofluid flow over a porous stretching/shrinking surface. Entropy, 2016;vol.18(4). http://dx.doi.org/10.3390/e18040123.

15. Khan MI, Waqas M, Hayat T, Alsaedi A. A comparative study of casson fluid with homogeneous-heterogeneous reactions. Journal of Colloid Interface Science. 2017; vol.(49):pg no.85–90.
http://dx.doi.org/10.1016/j.jcis.2017.03.024.

16. Loganathan P, Deepa K. Electromagnetic and radiativecasson fluid flow over a permeable vertical Riga-plate. J Theoretical Applied Mechanical. 2019; vol.(57):pg: 987–998. http: //dx.doi.org/10.15632/jtam-pl/112421.

17. Nadeem S, Ashiq S, Ali M. Williamson fluid model for the peristaltic flow of chyme in small intestine. Math Probl Eng. 2012;2012:479087. http://dx.doi.org/ 10.1155/2012/479087, 18 pages.

18. Khan NA, Khan S, Riaz F. Boundary layer flow of williamson fluid with chemically reactive species using scaling transformation and homotopy analysis method. Mathematical science letters. 2014;vol.(3)1,pg no:199-205. http://dx.doi.org/10.12785/msl/030311.

19. Hashim A, Khan M, Hamid A. Numerical investigation on time-dependent flow of williamsonnanofluid along with heat and mass transfer characteristics past a wedge geometry. International journal of Heat and Mass Transfer. 2018,vol.(118), pg:480–491. http://dx.doi.org/ 10.1016/j.ijheatmasstransfer.2017.10.126.

20. Shamshuddin MD, Mabood F, Salawu SO. Flow of three-dimensional radiativewilliamson fluid over an inclined stretching sheet with hall current and n^{th} order chemical reaction.. Heat Transfer. 202,.vol.21),pg no.:1–15. http://dx.doi.org/10.1002/ htj.22130.

21. Subbarayudu K, Suneetha S, Reddy PBA. The assessment of time dependent flow of williamson fluid with radiative blood flow against a wedge. Propulsion and Power Research. 2020; vol.9(1):pg:87–99. http://dx.doi.org/10.1016/j.jppr.2019.07.001.

22. Yusuf TA, Akaje TW, Salawu SO, Gbadeyan JA. Arrhenius activation energy effect on a stagnation point slippery MHD cassonnanofluid flow with entropy generation and melting heat transfer. Defect Diffus Forum. 2021;408:1–18. http: //dx.doi.org/10.4028/www.scientific.net/DDF.408.1.

23. Sakiadis, B.C. Boundary-layer behavior on continuous solid surfaces: I. Boundary-layer equations for two-dimensional and axisymmetric flow. *AIChE J.* **1961**, *7*, 26–28..

24. Khan, S.; Selim, M.M.; Khan, A.; Ullah, A.; Abdeljawad, T.; Ikramullah; Ayaz, M.; Mashwani, W.K. On the Analysis of the Non-Newtonian Fluid Flow Past a Stretching/Shrinking Permeable Surface with Heat and Mass Transfer. *Coatings* **2021**, *11*, 566.

25. Zeb, H.; Bhatti, S.; Khan, U.; Wahab, H.A.; Mohamed, A.; Khan, I. Impact of Homogeneous-Heterogeneous Reactions on Flow of Non-Newtonian Ferrofluid over a Stretching Sheet. *J. Nanomater.* **2022**, *2022*, 2501263.

26. Mahabaleshwar, U.S.; Maranna, T.; Sofos, F. Analytical investigation of an incompressible viscous laminar Casson fluid flow past a stretching/shrinking sheet. *Sci. Rep.* **2022**, *12*, 18404.

27. Abbas, N.; Nadeem, S.; Shatanawi, W. Effects of radiation and heat generation for non-Newtonian fluid flow over slendering stretching sheet: Numerically. *J. Appl. Math. Mech.* **2022**, *103*, e202100299.

28. Mohamed E. Ali. The Effect of Suction or Injection on the Laminar Boundary Layer Development Over a Stretched Surface. https://doi.org/10.1016/S1018-3639(18)30639-1.

29. M.Radhika, M.Anil kumar. Analysis of thermal radiation on MHD heat transfer in Williamson nanofluid flow over an exponentially porous stretching sheet with chemical reaction and slip effects. Journal of thermal analysis and calorimetry,jume 2025, vol 154{14). DOI:10.1007/s10973-025-14322-5

30. Chowdepalli, B., & Watanabe, K. (2023). Empirical equations expressing the effects of measured suction on the compaction curve for sandy soils varying fines content. *Geotechnics*, *3*(3), 760–780.

https://doi.org/10.3390/geotechnics3030042.

31. Iftikhar ahmed, Metib Alghamdi , Muhammad Amjad , Faisal Aziz , Tanvir Akbar , Taseer Muhammad. Numerical investigation of MHD flow of hyperbolic tangent nanofluid over a non-linear stretching sheet. *eliyon* **9**, 17658 (2023).

32. Reddy, M.G. Influence of magnetohydrodynamic and thermal radiation boundary layer flow of a nanofluid past a stretching sheet. *J. Sci. Res.* **2014**, *6*, 257–272.

33..Gnaneswara Reddy, M. Thermal radiation and chemical reaction effects on MHD mixed convective boundary layer slip flow in a porous medium with heat source and Ohmic heating. *EPJP* **2014**, *129*, 41.

34. AboEldahab, E.M. Radiation effect on heat transfer in an electrically conducting fluid at a stretching surface with a uniform free stream. *J. Phys. D Appl. Phys.* **2000**, *33*, 3180.

35..Abo-Eldahab, E.M.; El Gendy, M.S. Radiation effect on convective heat transfer in an electrically conducting fluid at a stretching surface with variable viscosity and uniform free stream. *Phys. Scr.* **2000**, *62*, 321. 36. Ahmed, I. et al. Numerical investigation of MHD flow of hyperbolic tangent nanofluid over a non-linear stretching sheet. Heliyon 9, e17658 (2023). DOI.10.1016/j.heliyon.2023.e17658.

37.W. Abbas , Ahmed M. Megahed . Eman Fares. The impact of a chemical reaction on the heat and mass transfer mechanisms in a dissipative and radiative nanofluid flow over a nonlinear stretching sheet. Scientific Reports,2024. https://doi.org/10.1038/s41598-024-57952-9